TR 253

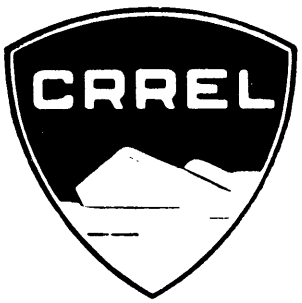

Technical Report 253

TRIAXIAL CONSTANT STRAIN RATE TESTS AND TRIAXIAL CREEP TESTS ON FROZEN OTTAWA SAND

Francis H. Sayles

August 1974

PREPARED FOR
DIRECTORATE OF MILITARY CONSTRUCTION
OFFICE, CHIEF OF ENGINEERS
BY
CORPS OF ENGINEERS, U.S. ARMY
COLD REGIONS RESEARCH AND ENGINEERING LABORATORY
HANOVER, NEW HAMPSHIRE

The findings in this report are not to be construed as an official Department of the Army position unless so designated by other authorized documents.

TRIAXIAL CONSTANT STRAIN RATE TESTS AND TRIAXIAL CREEP TESTS ON FROZEN OTTAWA SAND

Francis H. Sayles

August 1974

PREPARED FOR
DIRECTORATE OF MILITARY CONSTRUCTION
OFFICE, CHIEF OF ENGINEERS
BY
CORPS OF ENGINEERS, U.S. ARMY
COLD REGIONS RESEARCH AND ENGINEERING LABORATORY
HANOVER, NEW HAMPSHIRE

PREFACE

This report was prepared by Francis H. Sayles, Research Civil Engineer, Northern Engineering Research Branch, Experimental Engineering Division, U.S. Army Cold Regions Research and Engineering Laboratory. The study was conducted for the Directorate of Military Construction, Office of the Chief of Engineers. The program was under the technical direction of the Engineering Division of this directorate, Civil Engineering Branch.

The author is appreciative of assistance given by personnel in the testing laboratory. Specifically, thanks go to R. Bonnett, J. Ingersoll, A. Greatorex, D. May, J. Schweizer and J. Watts. The constructive comments on the final manuscript by E. Chamberlain and W. Quinn and Dr. G. Swinzow are gratefully acknowledged.

CONTENTS

ILLUSTRATIONS

TRIAXIAL CONSTANT STRAIN RATE TESTS AND TRIAXIAL CREEP TESTS ON FROZEN OTTAWA SAND

by

Francis H. Sayles

INTRODUCTION

Triaxial compression tests using a constant rate of applied strain and triaxial creep tests using a constant load were conducted on saturated frozen Ottawa sand (20-30 mesh) and ice to gain a better understanding of the factors that influence the strength and deformation characteristics of frozen soils. Several published results of conventional unconfined compression tests, direct shear tests and unconfined compression creep tests* show that the strength and deformation of a given frozen soil are strongly dependent upon temperature and duration of applied stress. Although Vyalov[10] discussed triaxial testing of frozen soil and suggested a generalized creep theory taking hydrostatic pressure into account, and Andersland and AlNouri[2] presented data from triaxial tests on Ottawa sand using confining pressures up to about 0.62×10^6 N/m^2 (90 psi), the influence of confining pressure and rate of loading on strength and deformation have not been fully assessed.

Strength and deformation of frozen soils, as with unfrozen cohesive soils, depend upon both the cohesion and the internal friction of the component materials. According to Vyalov and Tsytovich,[11] the cohesion component in frozen soils can be attributed to: 1) molecular forces of attraction between particles, 2) physical or chemical cementing of particles together, and 3) cementing of particles by ice formation in the soil voids. The cementation by ice is the result of the bonds between the ice crystals and the soil particles even though the soil particles are surrounded by a film of unfrozen water. This cementation implies that the unfrozen water under the influence of molecular forces of the soil particles is capable of transmitting normal and even some shear forces between the solid ice and the solid soil grains. The cohesion depends upon the amount, strength, and area of ice in contact with the soil particles, each of which is temperature dependent. The internal friction depends upon the ice content; the soil grain arrangement, size, distribution and shape; and the number of grain-to-grain contacts.[8 11] Except for the ice content, each of these factors is independent of temperature.

The purpose of this investigation was to study the effects of hydrostatic confining pressure and the rate of applied load on the strength and deformation characteristics of frozen sands and to assess the relative influence of the cohesion of the ice matrix versus the friction between the particles of sand.

---

* Refs. 1, 2, 4, 5, 7, 8, 9 and 12.

TEST PROCEDURE

The testing was conducted on cylindrical specimens about 70 mm (2.75 in.) in diameter and about 152.5 mm (6.0 in.) long. These dimensions were chosen to ensure a large ratio between specimen diameter and soil particle size and to use existing available testing apparatus. Each sand specimen was packed in a freezing mold, saturated with distilled, de-aired water under about 700 mm of mercury vacuum, then frozen from the top down in an open system where free water had access to the bottom of the specimen. The rate of progress of the 0°C (32°F) isotherm was determined by means of thermocouples spaced 25.4 mm (1 in.) apart along the vertical axis of a control specimen. Soil samples were frozen within a period of 4 days and the average rate of front penetration was about 38 mm (1½ in.) per day. No expansion of the specimens was observed during the freezing process. The increase in volume because of the change in phase of the water to ice was absorbed in the free water supply connected to the bottom of the specimen. The ice specimens used in this study were prepared in a manner similar to that of the sand. All specimens were trimmed to ensure that the ends were perpendicular to the axis and were enclosed in two and sometimes three rubber membranes to prevent the intrusion of the confining fluid (ethylene glycol and water). The Ottawa sand specimens were saturated and had an average dry unit weight of about 1670 kg/m^3 (104 lb/ft^3), a void ratio of about 0.59, and a porosity of 37%; and the specific gravity of the soil particles was 2.65. The average dry unit weight of the ice specimens was about 913 kg/m^3 (56.9 lb/ft^3). Values for each specimen are given in Tables AI and AII in the Appendix.

Nominal hydrostatic confining pressures σ_3 of 0.34×10^6 N/m^2 (50 psi) to 8.2×10^6 N/m^2 (1200 psi) were used; superimposed axial (deviator) stresses $(\sigma_1 - \sigma_3)$* in the creep tests were 0.525×10^6 N/m^2 (75 psi) to 6.89×10^6 N/m^2 (1000 psi); the test temperature was -3.85°C (25°F). In the compression tests the diameter of the specimen increased with axial deformation. The resulting axial stresses were computed on the assumption that the volume of the specimen remained constant and the specimen remained a cylinder throughout each test. These assumptions were consistent with visual observations.

TRIAXIAL TESTS AT CONSTANT STRAIN RATE

Laboratory data from the constant rate of strain tests show that the shape of the stress-strain curve and the maximum or peak stresses are governed by the rate of applied strain and the magnitude of the hydrostatic confining pressure. Stress-strain curves for a rate of applied strain of about 0.03/min are shown in Figure 1. Where strains exceed about 0.1, two peak stresses occur when the confining pressure σ_3 is above about 2.7×10^6 N/m^2 (400 psi). The first peak occurs at strains less than 0.01 and the second at a strain of about 0.1. The strain at which the first stress peak occurs is close to the strain at failure for columnar-grained ice specimens (i.e. where the ice crystals are columns with axes parallel to those of the cylinder specimen) also shown in Figure 1. This observation suggests that the first peak is essentially the consequence of the strength of the ice matrix and the second is the development of friction between grains of sand and/or ice crystals as the strain progresses. The frictional resistance increases until the maximum dilatancy of the sand grains is reached and the second peak in the stress-strain curve is attained.

Since the strength due to internal friction of the sand increases with confining pressure and for practical purposes the cohesion of an ice crystal does not, the second peak of the stress-strain

* $(\sigma_1 - \sigma_3)$ is the axial deviator stress where σ_1 is the major principal stress and σ_3 is the hydrostatic confining pressure.

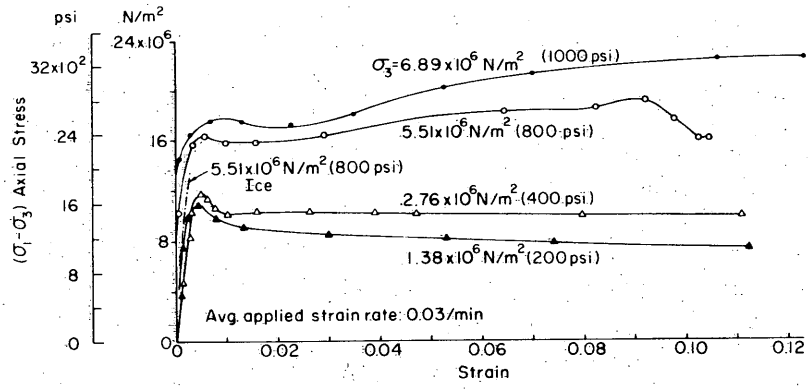

Figure 1. Axial stress-strain curves for Ottawa sand and ice at different confining pressures σ_3 and at large strains.

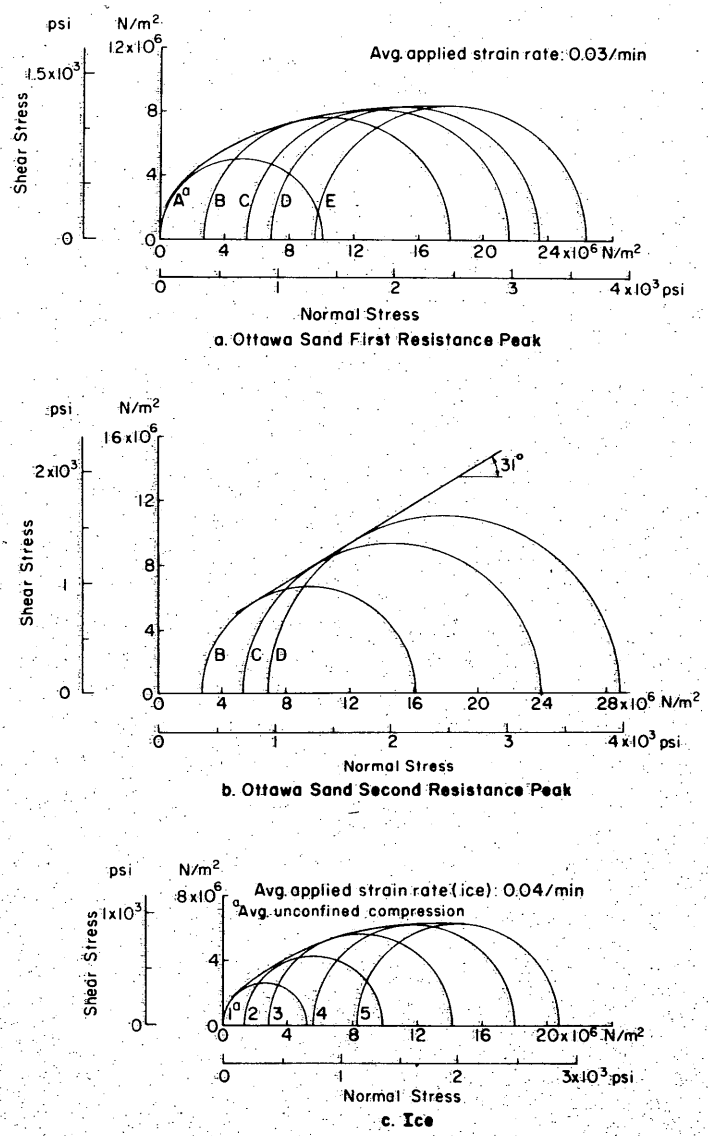

Figure 2. Mohr envelopes for Ottawa sand and ice. A-E and 1-5 on curves indicate different specimens of sand and ice.

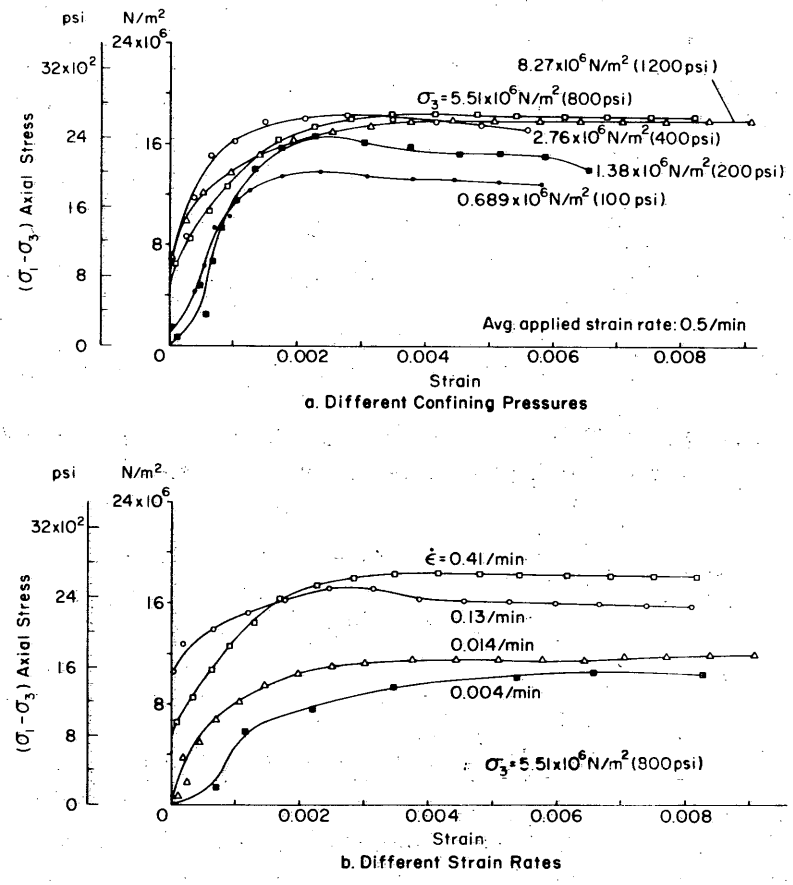

Figure 3. Axial stress-strain curves for Ottawa sand at small strains.

curve may be smaller than the first peak for low confining pressures and greater than the first peak for high confining pressures. In fact, it was observed, and is shown in Figure 1, that for confining pressure below 2.76×10^6 N/m² (400 psi) the frictional resistance might be considered as an apparent constant residual strength for each confining pressure.

The concept that each peak strength represents the domination of either the cohesive or frictional strength separately is reinforced by the two Mohr strength envelopes shown in Figure 2. The envelope in Figure 2b is nearly a straight line with an angle of internal friction of about 31°, a value similar to that of unfrozen Ottawa sand. The envelope in Figure 2a is curved for the lower values of confining pressure, indicating that there is some internal friction involved at these lower levels of confining pressures. However, this envelope approaches nearly a constant value at the higher confining pressures, suggesting that cohesion provides nearly all resistance at these confining pressures and small strains. The influence of confining pressure on the stress-strain curve for the first stress peak for the constant rate of applied strain of 0.5/min is shown in Figure 3a. The first peak stresses increase with confining pressure up to pressures of about 2.7×10^6 N/m² (400 psi), and above this value the confining pressure appears to have little influence on the strength.

The Mohr envelope for polycrystalline columnar-grained ice (Fig. 2c) also shows that for confining pressures below 2.7×10^6 N/m² (400 psi) the ice has a strength dependency on confining pressure and above 2.7×10^6 N/m² (400 psi) the strength of the ice is nearly independent of confining pressure. The curve is consistent with the concept that the first peak stress on the stress-strain curve is a reflection of the influence of the ice matrix of the soil.

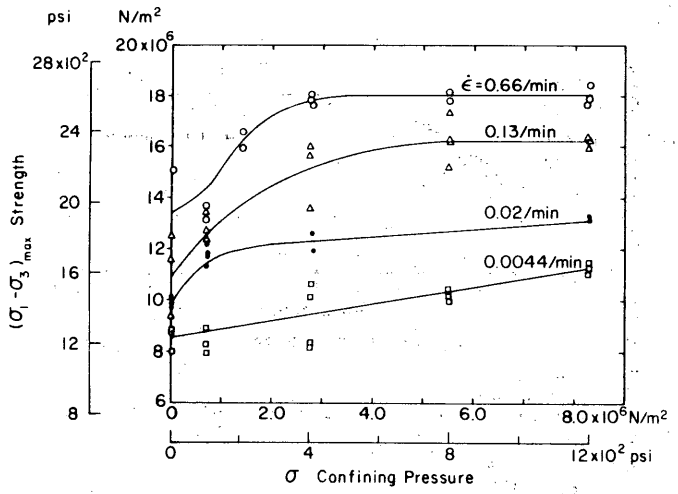

Figure 4. Strength vs confining pressure σ_3 for Ottawa sand.

The strength dependency of polycrystalline ice upon confining pressure below about 2.7×10^6 N/m² (400 psi) could be attributed to the friction between the individual ice crystals. As the confining pressure is increased above 2.7×10^6 N/m² (400 psi), the ice crystals are pressed together and tend to resist the applied stress as a combined single crystal. The nearly constant shearing strength of about 6.2×10^6 N/m² (900 psi) shown in Figure 2c is greater than the values reported[3] for a single ice crystal tested along the glide direction. This result is expected because it would be improbable for the glide planes of the crystals in the polycrystalline ice to have the same orientation and hence the same resistance to shear as a single crystal. Also to be noted in Figures 2a and 2c is the difference in Mohr envelopes, indicating that in samples of frozen sand some shearing resistance at the first peak of the stress-strain curve is contributed by the arrangement of sand grains.

The shapes of the stress-strain curves for the first resistance peak shown in Figure 3b suggest a plastic type of failure rather than a brittle failure ending in an abrupt fracture. These curves indicate that as the rate of applied strain increases the maximum peak resistance increases. It is questionable whether the resistance can increase indefinitely with the increase in strain rate before some other phenomenon such as brittle fracturing of the ice matrix limits the first peak resistance of the frozen sand.

As shown in Figure 4, the combined effect of increasing applied strain rate $\dot{\epsilon}$ and confining pressure on the first or cohesion peak strength shows that the peak strengths for rates of strain above about 0.02/min increase with confining pressure up to about 2.7×10^6 N/m² (400 psi), then appear to be independent of confining pressure. At the lower rates of strain (below 0.02/min) the strength increases with increase in confining pressure; this suggests that friction between the sand grains is being activated, possibly because the ice matrix is allowed time to creep from between the sand grains where the stress concentration is high, thus bringing more sand grains into closer contact and hence creating greater frictional resistance.

Mohr envelopes for the first resistance peak of frozen sand for different rates of applied axial strain are plotted in Figure 5. Figure 5 also shows the combined effect of rate of strain and confining pressure. Again, above a confining pressure of about 2.7×10^6 N/m² (400 psi) the slope of the envelope is small. The slopes of the envelopes at the higher confining pressure are greater for the lower strain rates, possibly reflecting the friction between the ice crystals as well as the friction between the soil grains that have crept closer together.

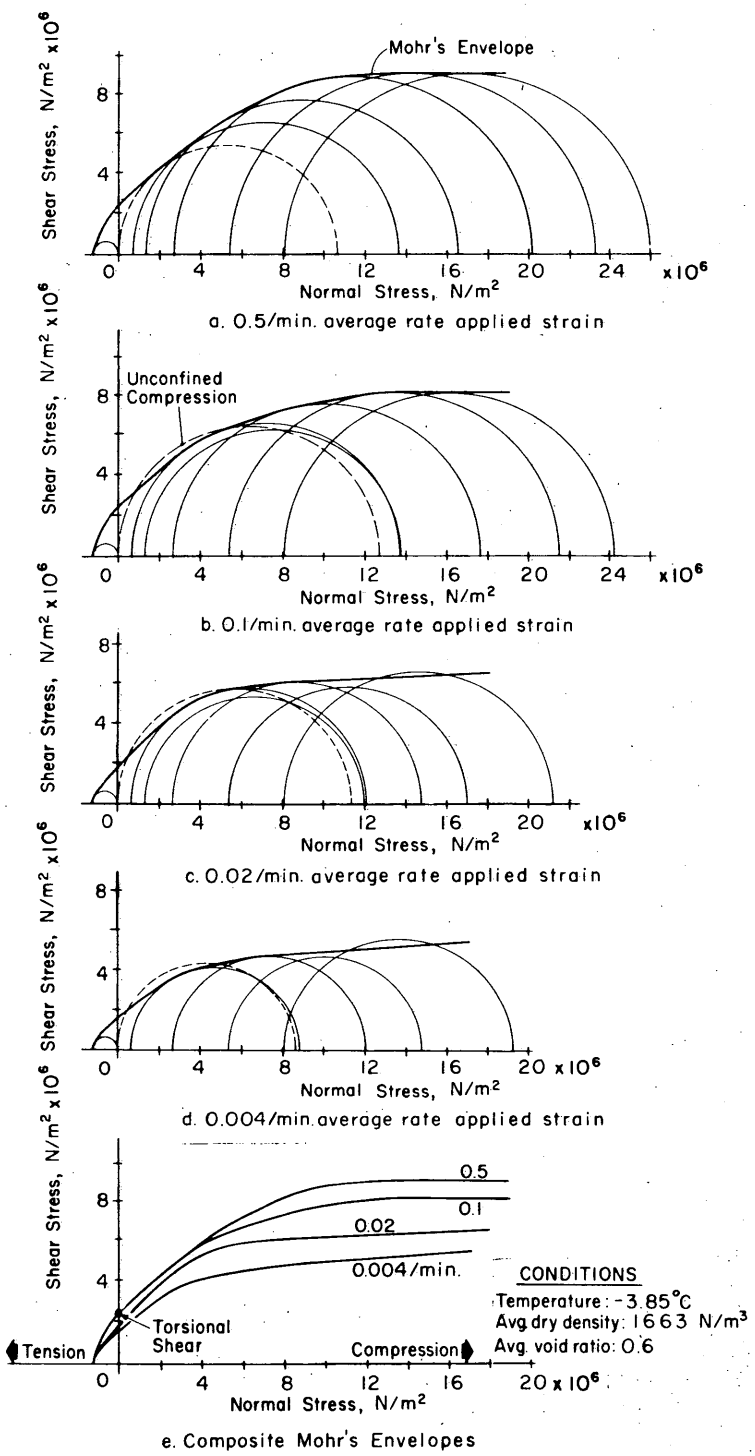

Figure 5. Mohr envelopes for Ottawa sand at different strain rates.

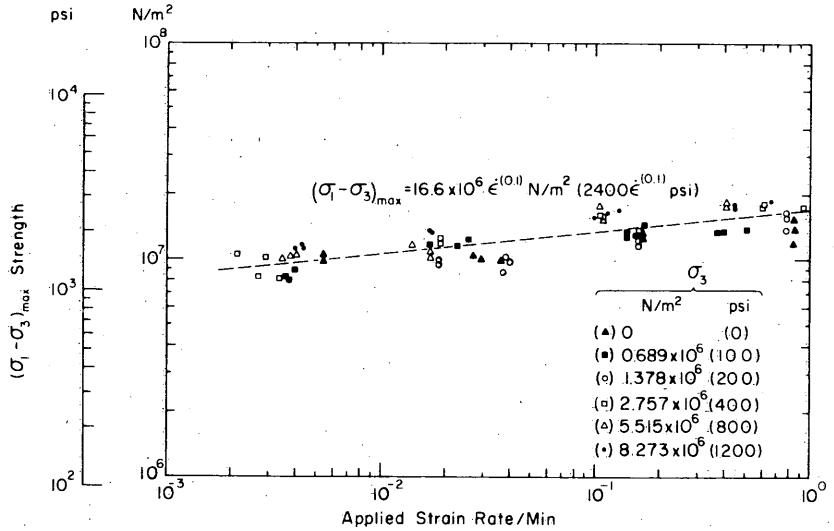

Figure 6. Strength vs applied strain rate for Ottawa sand.

There is evidence from unconfined compression tests that the strength of frozen Ottawa sand does not increase indefinitely as the rate of applied strain increases but is limited by a brittle type of failure at strain rates greater than 0.5/min. Nevertheless, the data obtained for confined compression in this investigation can be represented by the straight line shown in Figure 6 and the expression

$$(\sigma_1 - \sigma_3)_c = 16.6 \times 10^6 (\dot{\epsilon})^{0.1}$$

where $(\sigma_1 - \sigma_3)$ = first peak stress or strength in N/m²

$\dot{\epsilon}$ = applied rate of strain per minute.

This expression was derived using all constant applied strain rate test data obtained in this investigation and unconfined compression data from reference 5. Figure 6 is presented merely to show that the general trend is for the strength to increase as the rate of applied strain increases within the limits of the strain rates shown.

CREEP UNDER HYDROSTATIC STRESS CONFINING PRESSURE CONDITIONS

The time versus creep strain curves for constant confining pressures shown in Figure 7 summarize data from creep tests conducted in this investigation. Where more than one specimen was tested, a single curve represents the average for the specimens. The vertical bars on the curves give the total range of strain values at the location of the bar. The adjusted true strains were computed after accounting for the deformation of the test machine and the instantaneous deformation of the specimen by subtracting the initial deformation reading – the reading taken 5 seconds after application of the load. Since constant load tests were performed instead of constant stress tests, the strains were adjusted to a constant stress basis by assuming that the volume of the specimen remained constant and the specimen remained a cylinder throughout each test.

Although considerable care was taken to repeat each of the tests by preparing each specimen using the same process in every detail, by testing each replication under as nearly identical

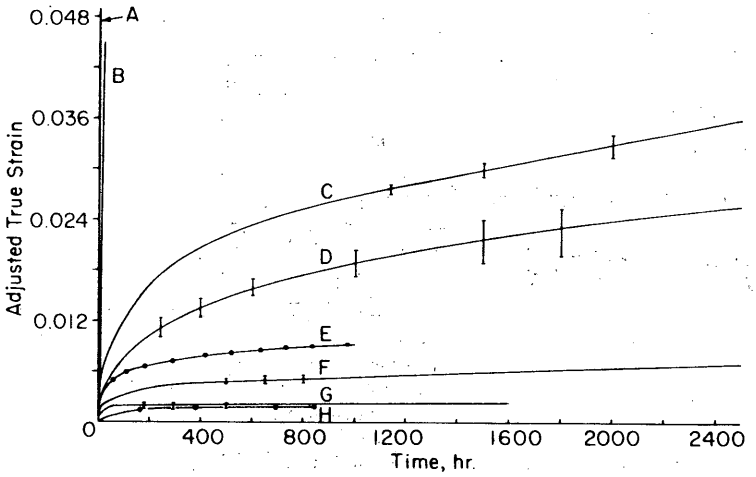

a.) $\sigma_3 = 0.345 \times 10^6$ N/m^2 (500 psi)

Curve	$\sigma_1 - \sigma_3$ N/m^2	$\sigma_1 - \sigma_3$ psi	OWS Specimen No's
A	4.13×10^6	600	468,471,473
B	2.76×10^6	400	487,479
C	1.72×10^6	250	262,266
D	1.38×10^6	200	350,567,571
E	0.69×10^6	100	553
F	0.517×10^6	75	352,319,337
G	0.345×10^6	50	562,375,376
H	0.108×10^6	15.6	374

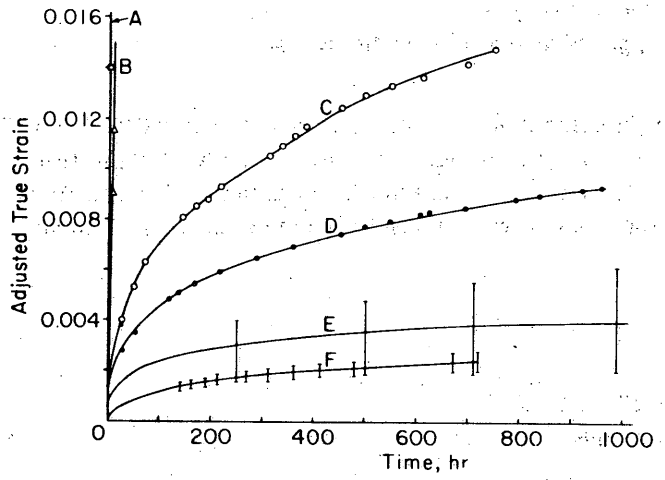

b.) $\sigma_3 = 0.517 \times 10^6$ N/m^2 (75 psi)

Curve	$\sigma_1 - \sigma_3$ N/m^2	$\sigma_1 - \sigma_3$ psi	OWS Specimen No's
A	4.13×10^6	600	466,472,476
B	2.76×10^6	400	482
C	1.38×10^6	200	463
D	1.03×10^6	150	391
E	0.517×10^6	75	392,461
F	0.256×10^6	37.2	424,429

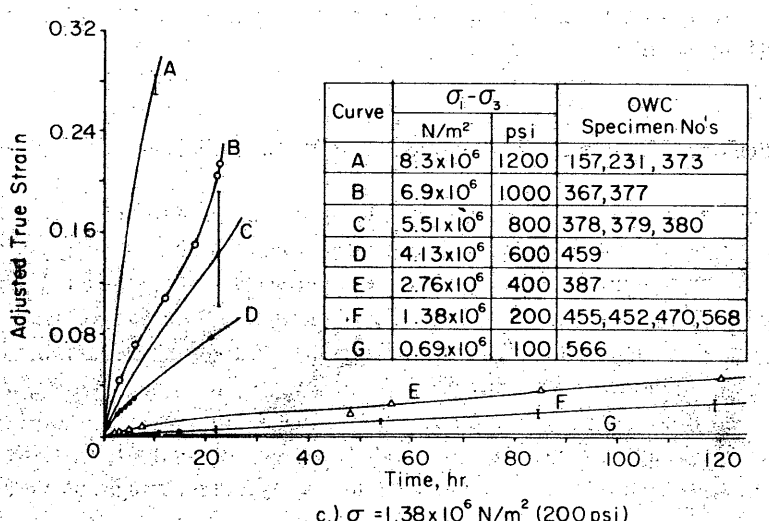

c.) $\sigma = 1.38 \times 10^6$ N/m^2 (200 psi)

Curve	$\sigma_1 - \sigma_3$ N/m^2	$\sigma_1 - \sigma_3$ psi	OWC Specimen No's
A	8.3×10^6	1200	157,231,373
B	6.9×10^6	1000	367,377
C	5.51×10^6	800	378,379,380
D	4.13×10^6	600	459
E	2.76×10^6	400	387
F	1.38×10^6	200	455,452,470,568
G	0.69×10^6	100	566

Figure 7. Summary creep curves for Ottawa sand at different confining pressures and axial stresses.

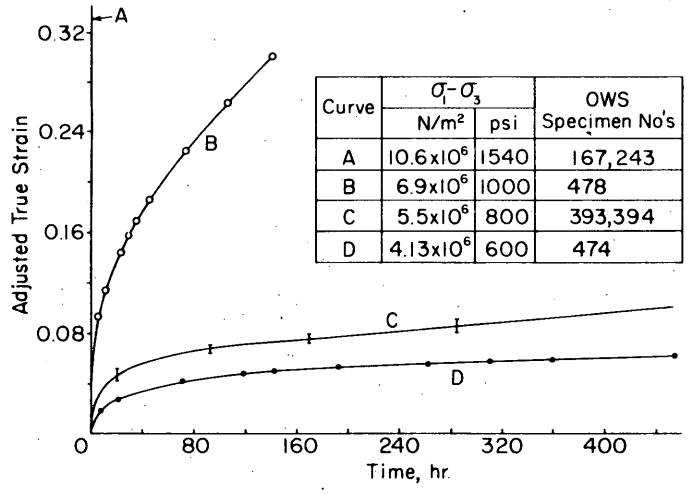

Curve	$\sigma_1-\sigma_3$ N/m²	$\sigma_1-\sigma_3$ psi	OWS Specimen No's
A	10.6×10^6	1540	167,243
B	6.9×10^6	1000	478
C	5.5×10^6	800	393,394
D	4.13×10^6	600	474

d.) $\sigma_3 = 2.76\times10^6$ N/m² (400 psi)

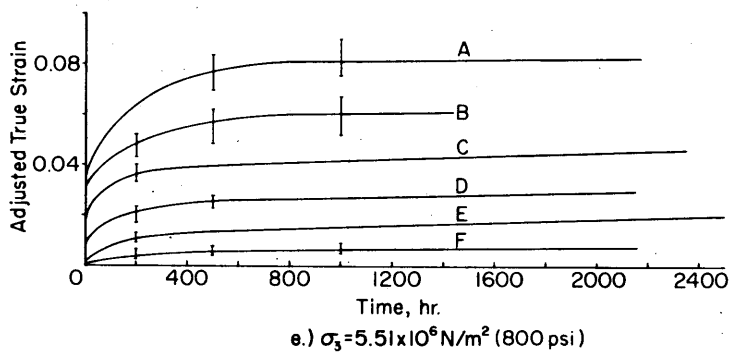

Curve	$\sigma_1-\sigma_3$ N/m²	$\sigma_1-\sigma_3$ psi	OWS Specimen No's
A	6.9×10^6	1000	499,500
B	5.51×10^6	800	511,518,535
C	4.13×10^6	600	539,521
D	2.76×10^6	400	538,525,540
E	1.38×10^6	200	505,515
F	0.69×10^6	100	534,545,552

e.) $\sigma_3 = 5.51\times10^6$ N/m² (800 psi)

Figure 7 (cont'd). Summary creep curves for Ottawa sand at different confining pressures and axial stresses.

conditions as possible, and by controlling the temperature within 0.1°C (0.18°F), there was considerable variation in the results, as shown by the size of the vertical bars on the summary creep curves. This variation is especially noticeable for the lower axial stress levels where the vertical bars overlap adjacent creep curves (Fig. 7a and b).*

As expected, these creep curves show that for a given confining pressure the magnitude of the strain at any given time increases with stress level. The effect of increasing the confining pressure is to reduce the amount of creep strain for a given period of constant axial stress application. This effect is demonstrated in Figure 8 where the axial stress is held constant and the confining pressure is increased. In comparing creep curves from triaxial tests with those from unconfined compression tests,[8] it was noticed that the first stage or primary creep was prolonged in the triaxial tests and that strains greater than 0.2 were reached without secondary creep being attained.

An examination of the various curves of this investigation at the lower stress levels indicates that the rate of strain decreases continuously with time in a manner suggesting that an empirical power function relationship between the rate of creep strain and time may exist. The logarithmic plots of strain versus time data in Figure 9 can be represented by a straight line and the expression:

* Confining pressures were applied about 24 hours before the axial load was applied.

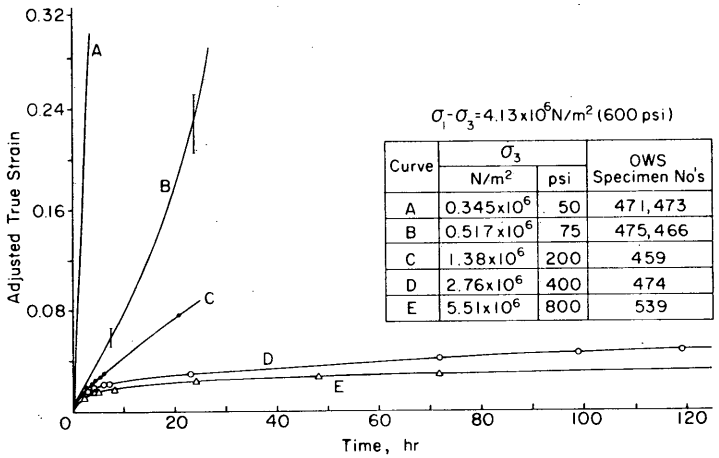

Curve	σ_3 N/m^2	σ_3 psi	OWS Specimen No's
A	0.345x10^6	50	471,473
B	0.517x10^6	75	475,466
C	1.38x10^6	200	459
D	2.76x10^6	400	474
E	5.51x10^6	800	539

Figure 8. Creep curves for Ottawa sand at constant axial stress ($\sigma_1 - \sigma_3$) and different confining pressures (σ_3).

Line	$\sigma_1-\sigma_3$ N/m	$\sigma_1-\sigma_3$ psi	OWS Specimen No.
A	1.0x10^6	145	391
B	0.517x10^6	75	496
C	0.26x10^6	37.5	424

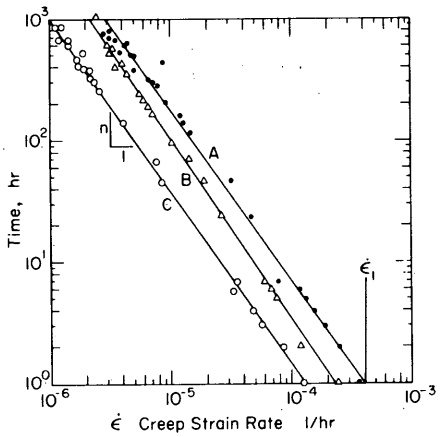

Figure 9. Time vs creep strain rate for Ottawa sand.

$$\dot{\epsilon}/\dot{\epsilon}_R = (t/t_R)^{1/n}$$

or

$$\dot{\epsilon} = [\dot{\epsilon}_R/(t_R)^{1/n}](t)^{1/n} \tag{1}$$

where $\dot{\epsilon}$ = rate of strain at any time t greater than zero
t_R = a reference time greater than zero
$\dot{\epsilon}_R$ = a corresponding strain rate
n = the slope of the straight line on the plot.

Any convenient value for a reference time t_R greater than zero can be selected. However, by selecting a value from the early portion of the curve, future rates of strain can be predicted. Often t_R taken as 1 hour is convenient; then $\dot{\epsilon}_R$ becomes $\dot{\epsilon}_1$ and

$$\dot{\epsilon} = \dot{\epsilon}_1 t^{1/n}.$$

To obtain an expression for strain at any time, eq 1 can be integrated.

$$\dot{\epsilon} = (d\epsilon/dt) = [\dot{\epsilon}_R/(t_R)^{1/n}](t)^{1/n} \qquad \begin{matrix} t_R > 0 \\ t > 0 \end{matrix}$$

$$\int_{\epsilon_r}^{\epsilon} d\epsilon = \dot{\epsilon}_R/(t_R)^{1/n} \int_{t_r}^{t} (t)^{1/n}\, dt$$

$$\epsilon - \epsilon_r = [\dot{\epsilon}_R/(t_R)^{1/n}][n/(n+1)][t^{(n+1)/n} - t_r^{(n+1)/n}] \tag{2}$$

$$\text{for } n \neq -1, \quad t_r > 0, \quad t_R > 0$$

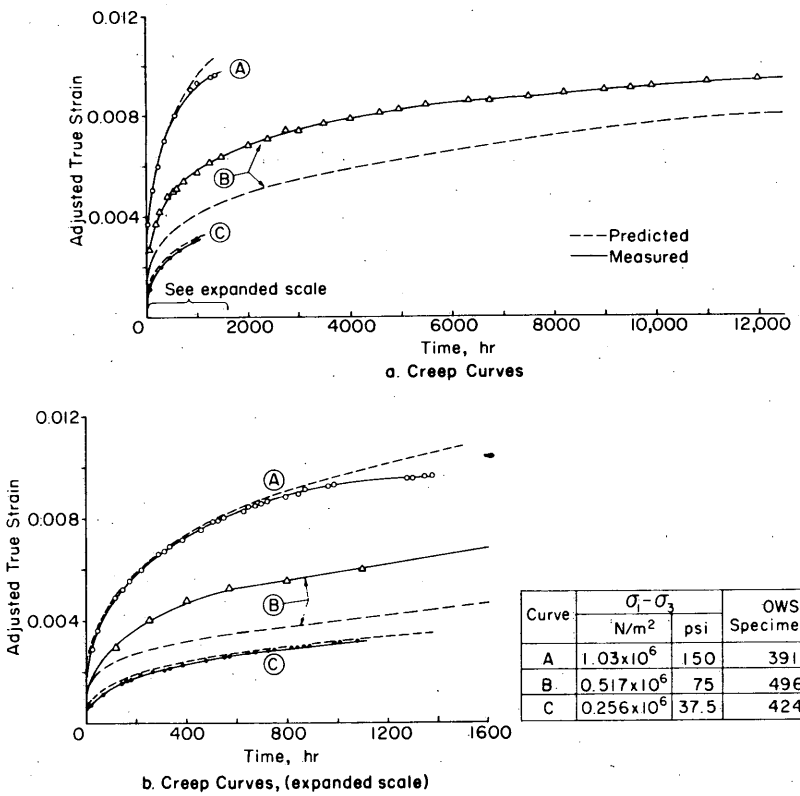

Curve	$\sigma_1-\sigma_3$ N/m²	$\sigma_1-\sigma_3$ psi	OWS Specimen No.
A	1.03×10^6	150	391
B	0.517×10^6	75	496
C	0.256×10^6	37.5	424

Figure 10. Measured compared with predicted creep strain for Ottawa sand. A, B and C indicate different specimens of sand.

and

$$\epsilon - \epsilon_r = \dot{\epsilon}_R/(t_R)^{1/n} \ln(t/t_r) \qquad \text{for } n = -1$$

where t_r and ϵ_r are convenient reference time greater than zero and corresponding strain.

For t_R and t_r taken as 1 hour, then $\dot{\epsilon}_R = \dot{\epsilon}_1$ and $\epsilon_r = \epsilon_1$, and eq 2 becomes

$$\epsilon = \epsilon_1(n/n+1)[t^{(n+1)/n} - 1] + \epsilon_1 \qquad \text{for } n \neq -1 \tag{2a}$$

and

$$\epsilon = \epsilon_1(\ln t) + \epsilon_1 \qquad \text{for } n = -1.$$

By determining values of $\dot{\epsilon}_1$, ϵ_1 and n from short term creep tests conducted under the desired stress and temperature conditions, eq 2a provides a means for estimating the value of strain at any time. Figure 10 gives a comparison between the predicted or estimated strain and laboratory creep test data. The constants for eq 2a were determined from the first eight hours of each creep test.

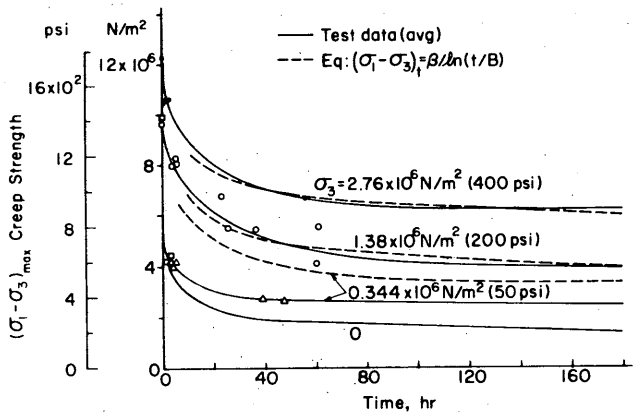

Figure 11. Creep strength vs time to failure for Ottawa sand.

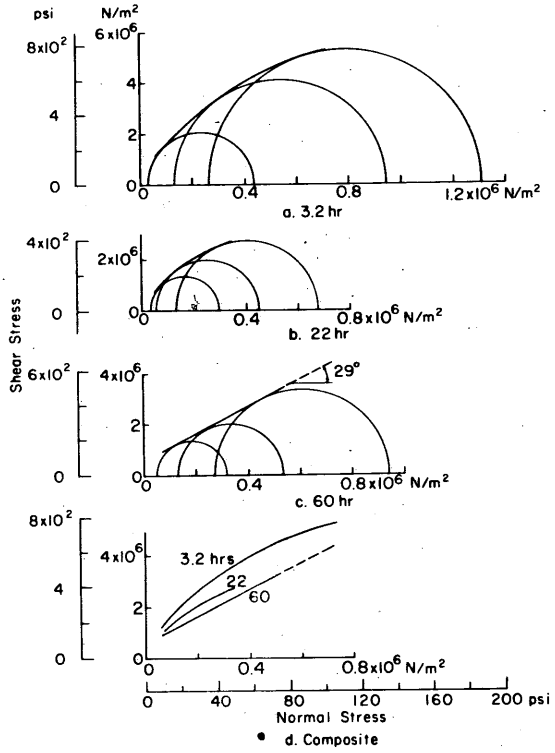

Figure 12. Mohr envelopes for creep strength of Ottawa sand.

TRIAXIAL CREEP STRENGTH

Since the soil tested in this investigation did not fail abruptly by rupture but instead deformed continuously in a plastic manner, the criterion for failure was arbitrarily taken to be the time the specimen strain reached 0.2. Assuming a strain of 0.2 as failure, strength vs time curves for different confining pressures were obtained by plotting the time to failure against the corresponding creep strength (Fig. 11). These curves are drawn to approach asymptotically the maximum test stresses that did not result in specimen failure during the test period. Although limited data are available for each confining pressure and the data vary somewhat, especially for confining pressures of 1.38×10^6 N/m² (200 psi), the test results can be represented by[10]

$$\sigma_t \cong (\sigma_1 - \sigma_3)_t \cong \beta/\ln (t/B) \tag{3}$$

where β and B are parameters that can be determined by short-term creep tests under the stress and temperature conditions for which estimated strengths are required. The strength variations with time predicted by eq 3 are represented by dashed lines in Figure 11 for comparison with the test data for relatively short creep tests.

Mohr envelopes representing creep strengths for different times after application of constant axial stress are shown in Figure 12. The curved envelopes for the shorter periods of time suggest that the strength of the ice crystals and the friction between the ice crystals dominate the strength of the soil mass much in the manner indicated in the constant rate of applied strain

tests previously described. The envelopes for the 60-hour period at reduced constant axial stress approach a straight line with an angle of internal friction of about 29°. As mentioned earlier, this angle is near that of unfrozen Ottawa sand, thus implying that friction between the sand grains dominates the strength of the soil mass at the longer test times. These envelopes suggest that at lower applied axial stresses, time is available for the ice to creep from between the sand grains and allow the development of an increase in the number of soil grain contacts and firmer grain-to-grain contacts. The frictional resistance of the sand grains would thus tend to dominate the strengths of the sand over long periods. It is hypothesized that the long term, ultimate creep strengths of frozen sands can be estimated by drained triaxial tests on sands under the same stress conditions and unit weights as those of the in-situ material. For practical purposes Mohr-Coulomb's expression

$$\tau = C + \sigma_n \tan\phi \tag{4}$$

where C = cohesion
σ_n = normal stress
ϕ = angle of internal friction for the sand

would apply.

It is emphasized that eq 4 should be applied only to sands with low ice contents and porosity of about 37% or less. Soils with high ice content and porosity can behave in a viscous manner.[6]

SUMMARY AND CONCLUSIONS

The results of this investigation based on triaxial compression tests performed on saturated frozen Ottawa sand (20-30 mesh) and polycrystalline columnar-grained ice at -3.85°C show that:

1. The resistance of saturated frozen Ottawa sand in a confined stress condition can be considered as consisting of the cohesion of the ice matrix and the frictional resistance of the sand grains. These sources of strength are nearly independent of each other when the applied rate of strain is greater than 0.02 min^{-1}. After the ice matrix has failed at a strain less than 0.01, the soil resistance becomes a function of the normal stress and the apparent angle of the internal friction of unfrozen sand, about 30°.

2. For a given temperature the initial or "cohesive" strength of the frozen sand increases with the rate of applied strain and can be represented approximately by the expression

$$(\sigma_1 - \sigma_3)_c = 16.6 \times 10^6 (\dot{\epsilon})^{0.1}$$

where $(\sigma_1 - \sigma_3)_c$ = initial or cohesive strength
$\dot{\epsilon}$ = applied strain rate from 0.002 to 1.0/min.

3. The rate of increase in the initial shear strength of saturated frozen Ottawa sand and polycrystalline columnar-grained ice decreases with increasing confining pressure. At the higher confining pressures used in this investigation, the initial shear strength is nearly independent of confining pressure at rates of applied strain greater than 0.02.

4. The short-term (periods of up to 100 hours) creep strength of frozen Ottawa sand can be represented by Vyalov's[10] strength equation:

$$\sigma_t \cong (\sigma_1 - \sigma_3)_t \cong \beta/\ln (t/B). \tag{3}$$

5. For low axial (deviator) stress levels, the creep strain rate can be represented by the empirical expression:

$$\dot{\epsilon}/\dot{\epsilon}_R = (t/t_R)^{1/n} \tag{1}$$

$$\dot{\epsilon} = [\dot{\epsilon}_R/t/R^{\ln}](+)^{1/n}$$

for a given constant stress and temperature condition.

6. For low axial (deviator) stress levels, creep strain can be estimated by

$$\epsilon - \epsilon_r = [\dot{\epsilon}_R/(t_R)^{1/n}][n/(n+1)][t^{(n+1)/n} - t_r^{(n+1)/n}] \qquad \text{for } n \neq -0,\ t_r > 0,\ t_R > 0 \tag{2}$$

and

$$\epsilon - \epsilon_r = \dot{\epsilon}_R/(t_R)^{1/n} \ln(t/t_r) \qquad \text{for } n = -1$$

for a constant stress and temperature condition. At higher axial stress levels where the creep curve approaches a straight line, clearly this equation is not applicable.

7. It is hypothesized that the long-term ultimate creep strength of saturated frozen sand with a porosity of 37% or less is a function of the angle of internal friction of the sand which could be determined through triaxial tests on freely drained unfrozen sand.

LITERATURE CITED

1. Andersland, O.B. and W. Akili (1967) Stress effect on creep rates of frozen clay. *Geotechnique*, vol. 17, p. 27-39.

2. Andersland, O.B. and I. AlNouri (1970) Time-dependent strength behavior of frozen soils. *Journal of Soil Mechanics and Foundations Division*, American Society of Civil Engineers (ASCE), vol. 96, no. SMA, p. 1249-1265.

3. Muguruma, J. (1969) Effects of surface condition on the mechanical properties of ice crystals. *British Journal of Applied Physics (Journal of Physics D)*, ser. 2, no. 11, p. 1517-1525.

4. Sanger, F.J. and C.W. Kaplar (1963) Plastic deformation of frozen soils in unconfined compression. *Proceedings, First Permafrost International Conference*, Building Research Advisory Board, National Academy of Sciences.

5. Sayles, F.H. (1968) Creep of frozen sands. U.S. Army Cold Regions Research and Engineering Laboratory (USA CRREL), Technical Report 190. AD 680902.

6. Thompson, E.G. and F.H. Sayles (1972) In-situ creep analysis of room in frozen soil. *Journal of Soil Mechanics and Foundations Division*, ASCE, vol. 98, no. SM9, Proc. Paper 9202, p. 899-915.

7. Tsytovich, N.A. and M.I. Sumgin (1957) Principles of mechanics of frozen ground. U.S. Army Snow, Ice and Permafrost Research Establishment (USA SIPRE), Translation 19 (out of print).

8. USA SIPRE (1952) Investigation of description, classification and strength properties of frozen soils. Prepared by U.S. Army Arctic Construction and Frost Effects Laboratory (USA ACFEL), U.S. Army Corps of Engineers for USA SIPRE, Report 8.

9. Vyalov, S.S. (1959) Rheological properties and bearing capacity of frozen soils. USSR Academy of Sciences. (Also USA SIPRE, Translation 74, 1963. AD 481856.)

10. Vyalov, S.S. (1963) Rheology of frozen soils. *Proceedings, First Permafrost International Conference*, Building Research Advisory Board, National Academy of Sciences.

11. Vyalov, S.S. and S. Tsytovich (1955) Cohesion of frozen soils. *Doklady Akademiia Nauk*, 104, no. 4, p. 527-529.

12. Young, R.N. (1963) Soil freezing consideration in frozen soil strength. *Proceedings, First Permafrost International Conference*, Building Research Advisory Board, National Academy of Sciences.

Table AI. Triaxial test – constant rate of applied strain, Ottawa sand (20-30).
Temperature = 25°F (-3.89°C)

Specimen number	Applied strain rate min^{-1}	Maximum axial stress $(\sigma_1 - \sigma_3)$ $N/m^2(\times 10^6)$	psi	γ_d N/m^3	γ_d lb/ft^3	γ_m N/m^3	γ_m lb/ft^3	V_I/V_S	S_I	e	Porosity	Water content	Tangent modulus @ 50% max. stress $\times 10^6$ psi	Tangent modulus @ 50% max. stress $\times 10^9$ N/m^2
σ_3 = 0.689 x 10^6 N/m^2 (100 psi)														
317	0.0036	8.30	1181	1635	102.1	1987	124.1	0.631	98.8	0.638	0.389	0.216	0.250	1.72
299*	0.0045	7.92	1147	1684	105.2	2043	127.6	0.622	105.6	0.590	0.371	0.213	0.227	1.56
288*	0.0050	9.00	1307	1645	102.7	2016	125.9	0.659	104.9	0.628	0.386	0.225	0.208	1.43
280*	0.017	11.78	1707	1643	102.6	2016	125.9	0.664	105.4	0.630	0.387	0.227	3.50	21.45
278*	0.023	11.30	1679	1652	103.2	2024	126.4	0.656	105.7	0.621	0.383	0.225	0.556	3.82
293*	0.026	12.18	1768	1673	104.5	2037	127.2	0.635	105.8	0.601	0.375	0.217		
281*	0.14	12.75	1845	1654	103.3	2021	126.2	0.647	104.4	0.618	0.382	0.221	0.818	5.64
295*	0.14	13.30	1928	1692	105.7	2040	127.4	0.601	103.2	0.582	0.368	0.206	0.708	4.88
264	0.16	12.40	1798	1661	103.7	2002	125.0	0.600	98.0	0.612	0.380	0.205	0.666	4.58
265	0.17	14.55	2107	1654	103.3	2000	124.4	0.611	98.7	0.619	0.382	0.209		
434	0.377	13.20	1920	1678	104.8	2015	125.8	0.583	98.8	0.590	0.371	0.200	4.76	32.8
435	0.399	13.20	1920	1672	104.4	2010	125.5	0.588	98.7	0.596	0.373	0.202	7.46	51.3
433	0.553	13.71	1990	1675	104.6	2013	125.7	0.587	99.0	0.592	0.372	0.201	2.00	13.8
σ_3 = 1.379 x 10^6 N/m^2 (200 psi)														
304*	0.0182	9.75	1411	1600	99.9	1984	123.9	0.701	104.2	0.673	0.402	0.240	0.263	1.81
308	0.0182	9.85	1425	1616	100.9	1974	124.5	0.655	99.6	0.658	0.397	0.224	0.270	1.86
313	0.0372	8.75	1265	1620	101.3	1979	123.0	0.648	49.3	0.653	0.395	0.192	0.192	1.32
303	0.038	10.15	1571	1621	101.2	1978	123.5	0.644	48.8	0.652	0.395	0.220	0.333	2.29
298*	0.040	9.7	1404	1606	100.3	1986	124.0	0.091	103.5	0.668	0.400	0.236	0.277	1.91
297	0.162	12.65	1836	1638	102.3	1991	124.3	0.627	98.8	0.634	0.388	0.214	0.323	2.22
316	0.163	12.2	1775	1638	102.3	1929	124.2	0.628	98.7	0.635	0.388		0.327	2.25
314	0.164	11.8	1716	1662	103.8	2005	125.2	0.601	98.4	0.611	0.379	0.206	0.323	2.22
414	0.770	13.85	2010	1656	103.4	2002	125.0	0.605	98.2	0.611	0.379	0.208	2.09	14.42
410	0.772	15.98	2310	1690	105.5	2007	125.3	0.547	94.4	0.579	0.367	0.188	3.31	22.85
416	0.772	16.62	2420	1634	102.0	1970	123.0	0.600	94.8	0.634	0.388	0.206	2.22	15.42
σ_3 = 2.758 x 10^6 N/m^2 (400 psi)														
321	0.00216	10.65	1555	1680	104.9	2017	126.0	0.588	98.9	0.594	0.373	0.201	0.195	1.34
323†	0.00268	8.40	1220											
305	0.00295	10.15	1475	1651	103.1	1998	124.8	0.614	98.9	0.621	0.383	0.210	0.2786	1.92
310	0.0034	8.20	1175	1645	102.7	1997	124.7	0.625	99.5	0.628	0.386	0.214	0.1045	0.72
307	0.019	11.9	1233	1622	101.3	1983	123.8	0.649	99.7	0.651	0.394	0.222	0.3091	2.13
311*	0.0192	12.6	1829	1588	99.2	1987	124.1	0.732	106.9	0.685	0.407	0.251	0.287	1.98
412*	0.105	16.0	2320	1634	102.1	2002	125.0	0.655	102.7	0.638	0.390	0.224	3.50	21.45
411	0.110	15.7	2284	1654	103.3	2003	125.1	0.618	99.8	0.619	0.382	0.211	No Data	
320	0.160	13.65	1988	1659	103.6	2005	125.2	0.609	99.3	0.614	0.380	0.209	0.30	2.07
413	0.608	18.0	2610	1670	104.3	2008	125.4	0.591	98.8	0.598	0.374	0.203	1.72	11.84
417	0.610	17.7	2570	1664	103.9	2005	125.2	0.598	99.0	0.604	0.376	0.205	Machine Error	
415	0.956	17.9	2600	1651	103.1	1992	124.4	0.605	98.2	0.616	0.381	0.208	1.692	11.64
σ_3 = 5.516 x 10^6 N/m^2 (800 psi)														
449	0.0035	10.0	1450	1675	104.6	2011	125.6	0.585	98.7	0.593	0.372	0.201	0.500	3.43
446	0.0038	10.45	1520	1777	111.0	2017	126.0	0.392	98.4	0.500	0.334	0.135	0.905	6.23
438	0.0040	10.45	1520	1677	104.7	2013	125.7	0.586	99)0	0.592	0.372	0.201	0.583	4.01
450	0.00402	10.45	1520	1683	105.1	2017	126.0	0.578	98.8	0.585	0.369	0.199	0.860	5.90
428	0.014	11.70	1700	1669	104.2	2008	125.4	0.591	98.8	0.598	0.374	0.203	0.660	4.54

* Error in weighing.
† Sample destroyed.
γ_d = dry unit weight; γ_m = mass unit weight; V_I/V_S = vol. of ice/vol. of soil grains; S_I = percent of voids filled with ice, e = void ratio.

Table AI (cont'd). Triaxial test – constant rate of applied strain, Ottawa sand (20-30).
Temperature = 25°F (-3.89°C)

Specimen number	Applied strain rate min^{-1}	Maximum axial stress $(\sigma_1 - \sigma_3)$ $N/m^2(\times 10^6)$	psi	γ_d N/m^3	γ_d lb/ft^3	γ_m N/m^3	γ_m lb/ft^3	V_I/V_S	S_I	e	Porosity	Water content	Tangent modulus @ 50% max. stress $\times 10^6$ psi	Tangent modulus @ 50% max. stress $\times 10^9$ N/m^2
σ_3 = 5.516 x 10^6 N/m^2 (800 psi) (cont'd)														
427	0.017	10.00	1460	1661	103.2	2003	125.1	0.599	98.8	0.606	0.377	0.206	0.951	6.55
430	0.017	10.90	1580	1672	104.4	2011	125.6	0.591	99.1	0.596	0.373	0.203	0.642	4.43
420	0.105	17.40	2520	1664	103.9	2007	125.3	0.598	99.2	0.603	0.376	0.205	1.386	9.59
419	0.109	15.20	2210	1662	103.8	2005	125.2	0.598	98.9	0.605	0.377	0.205	1.4	9.66
421	0.130	16.20	2350	1668	104.1	2008	125.4	0.596	99.2	0.600	0.375	0.205	1.372	9.49
425	0.407	17.8	2590	1670	104.3	2009	125.5	0.595	98.4	0.605	0.377	0.204	1.310	9.00
423	0.409	18.22	2650	1664	103.9	2007	125.3	0.598	99.2	0.602	0.376	0.205	1.058	7.29
σ_3 = 8.26 x 10^6 N/m^2 (1200 psi)														
445*	0.00399	11.20	1630	1598	99.8	2016	125.9	0.763	113.0	0.676	0.403	0.261	0.590	4.05
441	0.00432	11.0	1600	1678	104.8	2015	125.8	0.584	98.9	0.590	0.371	0.200	1.660	11.20
442	0.00433	11.55	1675	1677	104.7	2011	125.6	0.582	98.4	0.592	0.372	0.200		
437	0.017	13.3	1930	1678	104.8	2015	125.8	0.581	98.6	0.589	0.371	0.200	0.732	5.05
432	0.017	13.3	1930	1686	105.3	2019	126.1	0.573	98.5	0.582	0.368	0.197	0.864	5.96
440	0.099	15.95	2310	1682	105.0	2015	125.8	0.577	98.3	0.587	0.370	0.198	1.082	7.45
443	0.114	16.25	2360	1670	104.3	2010	125.5	0.586	98.4	0.595	0.373	0.201	0.895	6.18
439	0.130	16.35	2410	1672	104.4	2010	125.5	0.590	99.0	0.596	0.374	0.203	1.082	7.45
407†	0.444	17.8	2590											
448	0.444	17.9	2600	1661	103.2	2011	125.6	0.616	100.0	0.612	0.380	0.211	2.780	19.20
444	0.666	18.5	2690	1682	105.0	2016	125.9	0.578	98.7	0.586	0.370	0.199		

* Error in weighing.
† Sample destroyed.
γ_d = dry unit weight; γ_m = mass unit weight; V_I/V_S = vol. of ice/vol. of soil grains; S_I = percent of voids filled with ice, e = void ratio.

Table AII. Triaxial creep tests, Ottawa sand (20-30).
Temperature = 25°F (-3.89°C)

Specimen number	Maximum axial stress $(\sigma_1 - \sigma_3)$ N/m^2 $(\times 10^6)$	psi	γ_d N/m^3	γ_d lb/ft^3	γ_m N/m^3	γ_m lb/ft^3	V_I/V_S	S_I	e	Porosity	Water content
σ_3 = 2.758 x 10^6 N/m² (400 psi)											
389	11.03	1600	1648	102.9	2003	125.1	0.628	101.4	0.619	0.382	0.216
478*	6.894	1000									
394	5.516	800	1678	104.8	2016	125.9	0.585	99.4	0.589	0.371	0.201
393	5.516	800	1664	103.9	2013	125.7	0.614	100.7	0.609	0.379	0.210
474	4.14	600	1647	102.8	1995	124.6	0.618	99.6	0.621	0.383	0.212
454	2.758	400	1682	105.0	2016	125.9	0.579	98.7	0.586	0.370	0.199
σ_3 = 1.379 x 10^6 N/m² (200 psi)											
373	8.26	1200	1657	103.5	1995	124.6	0.595	97.5	0.610	0.379	0.204
231	8.26	1200	1624	101.6	2015	125.8	0.692	108.2	0.640	0.390	0.222
157	8.26	1200	1710	106.9	2035	127.1	0.553	98.0	0.569	0.361	0.189
153*	8.26	1200									
377	6.894	1000	1659	103.6	1998	124.8	0.596	98.0	0.608	0.378	0.205
267	6.894	1000	1626	101.7	2008	125.4	0.679	106.3	0.639	0.390	0.233
380†	5.516	800									
379	5.516	800	1652	103.2	1997	124.7	0.607	98.7	0.614	0.381	0.208
378	5.516	800	1640	102.4	1995	124.6	0.629	100.5	0.626	0.385	0.216
387	2.758	400	1662	103.8	2008	125.4	0.603	101.6	0.593	0.372	0.209
470	1.378	200	1634	102.0	1997	124.7	0.646	102.1	0.633	0.388	0.222
568*	1.379	200									
566	0.689	100	1785	111.5	2003	125.1	0.355	71.83	0.494	0.331	0.122
σ_3 = 0.51 x 10^6 N/m² (75 psi)											
476	4.14	600	1668	104.1	1998	124.8	0.579	96.4	0.601	0.375	0.199
472	4.14	600	1651	103.1	1997	124.7	0.612	99.3	0.616	0.381	0.210
466	4.14	600	1666	104.0	1998	124.8	0.583	96.8	0.602	0.376	0.200
482	2.758	400	1649	103.0	1995	124.6	0.611	98.9	0.618	0.382	0.210
465	1.378	200	1670	104.3	1998	124.8	0.573	95.8	0.598	0.374	0.197
391	1.35	150	1684	105.2	2017	126.0	0.574	98.4	0.583	0.368	0.197
461	0.517	75	1669	104.2	1992	124.4	0.565	94.3	0.599	0.375	0.194
392	0.517	75	1680	104.9	2015	125.8	0.578	98.4	0.588	0.370	0.199
463	1.378	200	1678	104.8	1997	124.7	0.551	93.5	0.589	0.371	0.189
496	0.517	75	1657	103.5	2004	125.2	0.610	100.10	0.609	0.379	0.210
429	0.258	375	1672	104.4	2008	125.4	0.585	98.2	0.596	0.374	0.201
424	0.258	375	1735	108.2	2002	125.0	0.453	83.9	0.540	0.351	0.156
σ_3 = 0.3447 x 10^6 N/m² (50 psi)											
473	4.14	600	1661	103.7	1998	124.8	0.594	97.9	0.607	0.378	0.204
471	4.14	600	1657	103.5	1995	124.6	0.595	97.5	0.610	0.379	0.204
487	2.758	400	1672	104.4	1998	124.8	0.570	95.6	0.596	0.373	0.196
479	2.758	400	1662	103.8	2008	125.4	0.604	99.8	0.605	0.377	0.207
266	1.72	250	1670	104.3	1998	124.8	0.577	95.45	0.604	0.377	0.197
262†	1.72	250									
350	1.378	200	1654	103.3	1998	124.8	0.604	98.6	0.613	0.380	0.207
571	1.379	200	1668	104.2	2000	124.9	0.579	96.68	0.599	0.374	0.199
567	1.379	200	1641	102.5	1961	122.5	0.568	90.83	0.625	0.385	0.195
553	0.689	100	1686	105.3	2001	125.0	0.545	93.67	0.582	0.368	0.187
352	0.517	75	1661	103.7	2000	124.9	0.595	98.2	0.606	0.377	0.204

* Weighing error.
† Sample destroyed.
γ_d = dry unit weight; γ_m = mass unit weight; V_I/V_S = vol. of ice/vol. of soil grains; S_I = percent of voids filled with ice; e = void ratio.

Table AII (cont'd). Triaxial creep tests, Ottawa sand (20-30).
Temperature = 25°F (-3.89°C)

Specimen number	Maximum axial stress ($\sigma_1 - \sigma_3$) N/m^2 ($\times 10^6$)	psi	γ_d N/m^3	γ_d lb/ft^3	γ_m N/m^3	γ_m lb/ft^3	V_I/V_S	S_I	e	Porosity	Water content
σ_3 = 0.3447 x 10^6 N/m² (50 psi) (cont'd)											
319	0.517	75	1645	102.7	1997	124.7	0.625	99.5	0.628	0.386	0.214
376	0.345	50	1668	104.1	2002	125.0	0.586	97.5	0.601	0.375	0.201
375	0.345	50	1668	104.1	2002	125.0	0.584	97.4	0.600	0.375	0.201
562	0.345	50	1646	102.8	2000	124.9	0.626	100.86	0.620	0.383	0.215
374	0.258	375	1664	103.9	1998	124.8	0.585	97.1	0.603	0.376	0.201
468	4.14	600	1662	103.8	1947	124.7	0.585	96.8	0.605	0.377	0.201
457	1.72	250	1648	102.9	1963	122.6	0.556	89.9	0.619	0.382	0.191
315	1.378	200	1652	103.2	1997	124.7	0.611	98.4	0.621	0.383	0.209
σ_3 = 2.758 x 10^6 N/m² (400 psi)											
477	7.46	1077	1634	102.0	1984	123.9	0.623	98.5	0.633	0.387	0.214
418	5.516	800	1643	102.6	2008	125.4	0.585	98.2	0.596	0.374	0.222
462	4.14	600	1637	102.2	1986	124.0	0.621	98.6	0.630	0.386	0.213
431	2.758	400	1678	104.8	2019	126.1	0.591	100.4	0.589	0.371	0.203
248	1.01	148	1710	106.5	2023	126.3	0.544	95.4	0.570	0.363	0.186
σ_3 = 5.515 x 10^6 N/m² (800 psi)											
499	6.93	1005	1655	103.4	1985	124.0	0.581	95.06	0.611	0.379	0.200
500	6.89	1000	1654	103.3	2000	124.9	0.606	99.06	0.612	0.380	0.208
511	5.515	800	1683	105.1	2000	124.9	0.547	93.63	0.585	0.369	0.188
518	5.515	800	1659	103.6	1984	123.9	0.570	93.66	0.608	0.378	0.196
535	5.46	792	1649	103.0	1963	122.6	0.557	90.04	0.618	0.382	0.191
539	4.14	600	1655	103.4	1985	124.0	0.582	95.11	0.612	0.380	0.200
538	2.76	400	1651	103.1	1982	123.8	0.587	95.12	0.617	0.381	0.201
525	2.76	400	1673	104.5	1993	124.5	0.558	98.89	0.594	0.373	0.192
505*	1.379	200									
515*	1.379	200									
545*	0.689	100									
534	0.676	98	1651	013.1	1996	124.7	0.609	98.90	0.616	0.381	0.209

* Weighing error.
† Sample destroyed.
γ_d = dry unit weight; γ_m = mass unit weight; V_I/V_S = vol. of ice/vol. of soil grains; S_I = percent of voids filled with ice; e = void ratio.

APPENDIX B: TRIAXIAL TEST STRESS-STRAIN CURVES

Saturated frozen Ottawa sand (20-30 mesh) at 25°F (-3.89°C). Confining pressures (σ_3) range from 100 to 1200 psi. Rates of applied strain range from .002 to 1.67 min.$^{-1}$

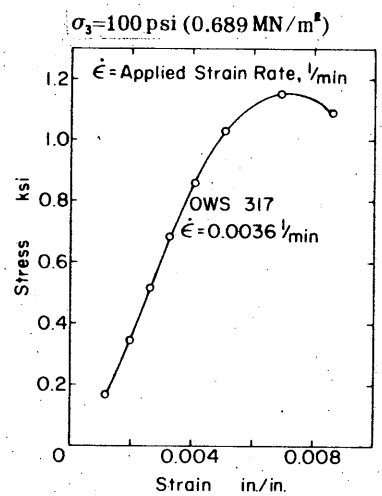

B1.

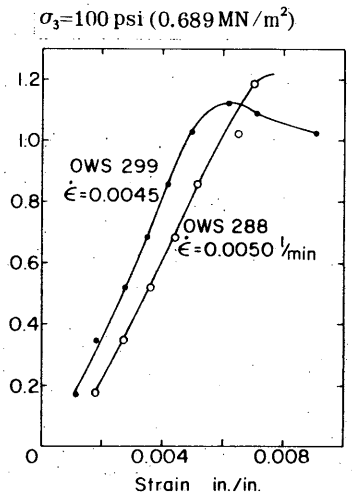

B2.

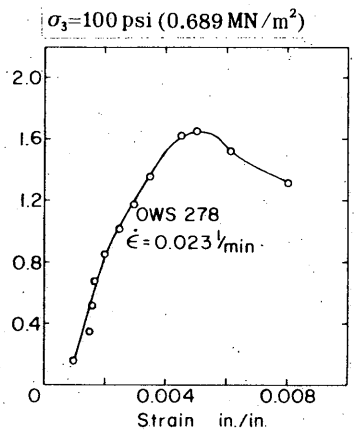

B3.

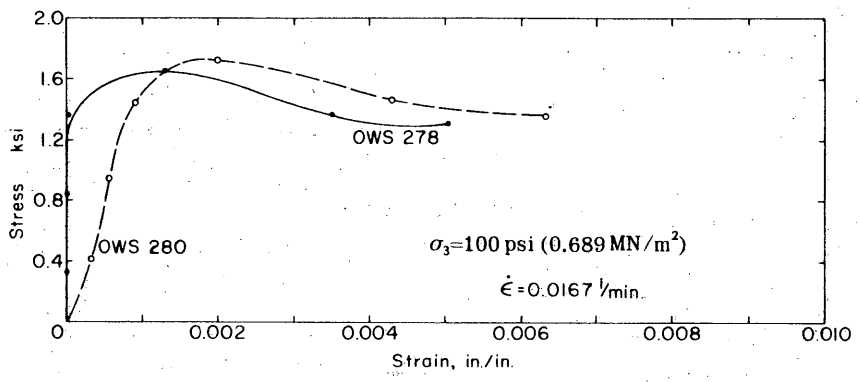

B4.

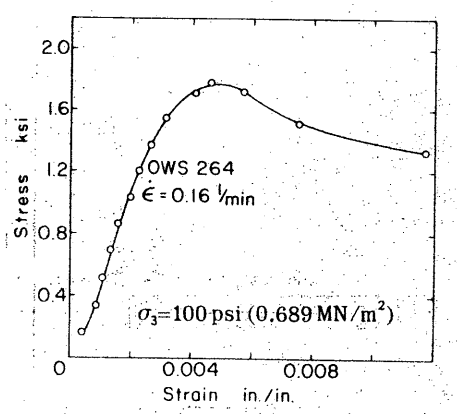

B5.

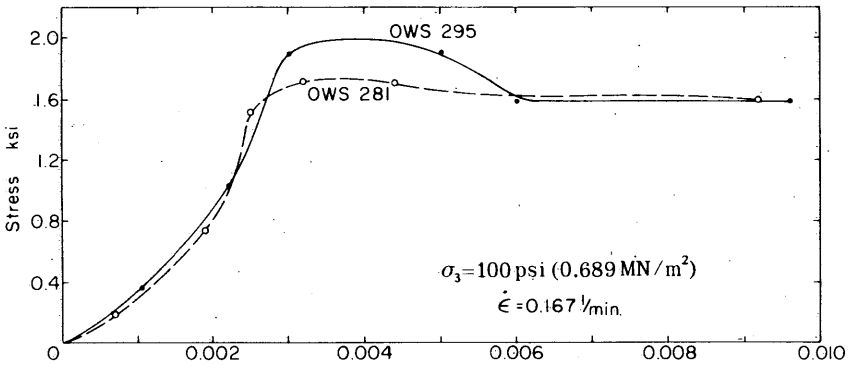
OWS 295
OWS 281
Stress ksi
2.0
1.6
1.2
0.8
0.4
0
0.002
0.004
0.006
0.008
0.010
σ_3=100 psi (0.689 MN/m^2)
$\dot{\epsilon}$ =0.167 1/min.

B6.

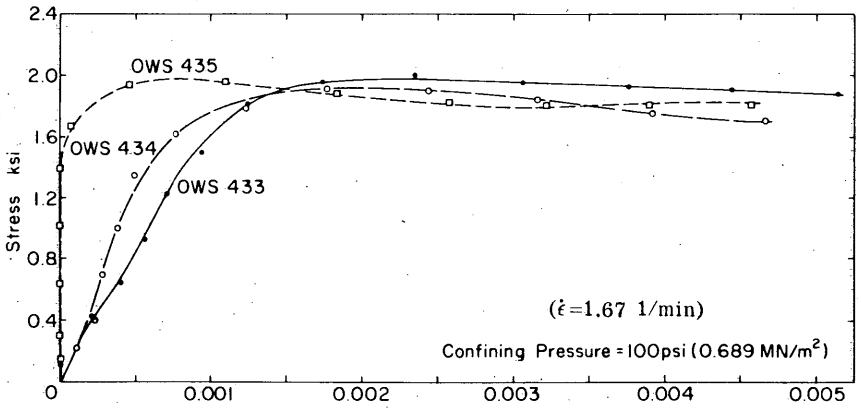
OWS 435
OWS 434
OWS 433
Stress ksi
2.4
2.0
1.6
1.2
0.8
0.4
0
0.001
0.002
0.003
0.004
0.005
($\dot{\epsilon}$=1.67 1/min)
Confining Pressure = 100psi (0.689 MN/m^2)

B7.

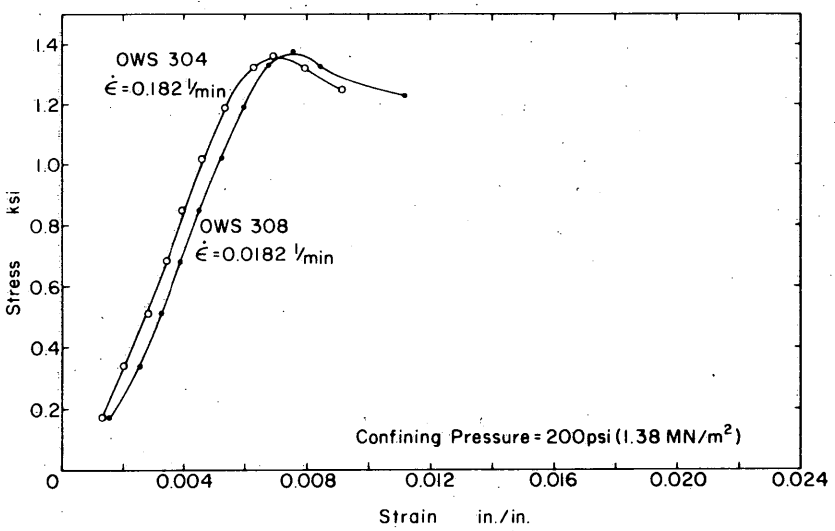
OWS 304
$\dot{\epsilon}$ =0.182 1/min
OWS 308
$\dot{\epsilon}$ =0.0182 1/min
Stress ksi
1.4
1.2
1.0
0.8
0.6
0.4
0.2
0
0.004
0.008
0.012
0.016
0.020
0.024
Strain in./in.
Confining Pressure = 200psi (1.38 MN/m^2)

B8.

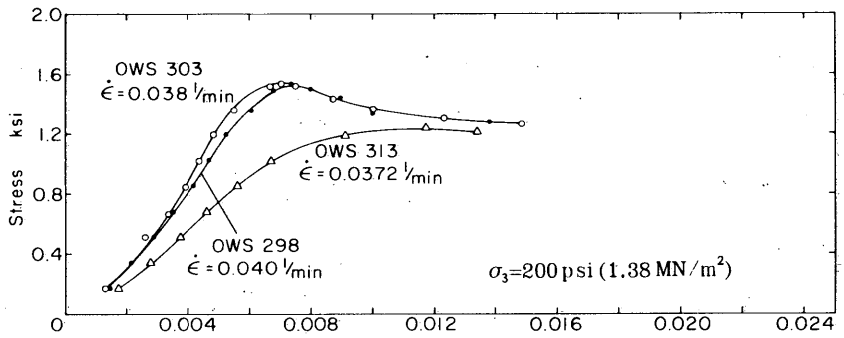
OWS 303
$\dot{\epsilon}$=0.038 1/min
OWS 313
$\dot{\epsilon}$=0.0372 1/min
OWS 298
$\dot{\epsilon}$=0.040 1/min
σ_3=200 psi (1.38 MN/m^2)
Stress ksi
2.0
1.6
1.2
0.8
0.4
0
0.004
0.008
0.012
0.016
0.020
0.024

B9.

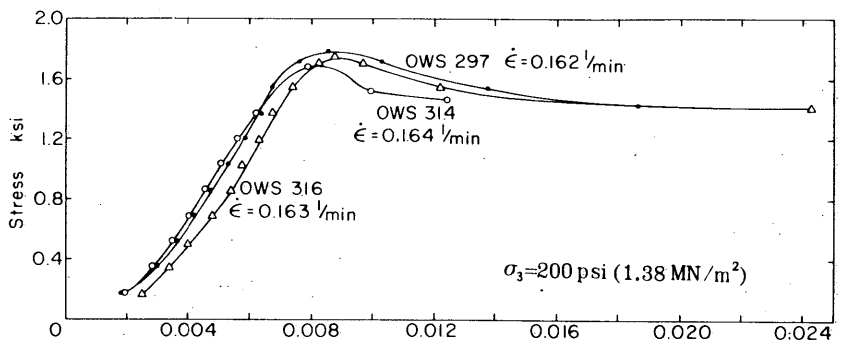
OWS 297 $\dot{\epsilon}$=0.162 1/min
OWS 314
$\dot{\epsilon}$=0.164 1/min
OWS 316
$\dot{\epsilon}$=0.163 1/min
σ_3=200 psi (1.38 MN/m^2)
Stress ksi
2.0
1.6
1.2
0.8
0.4
0
0.004
0.008
0.012
0.016
0.020
0.024

B10.

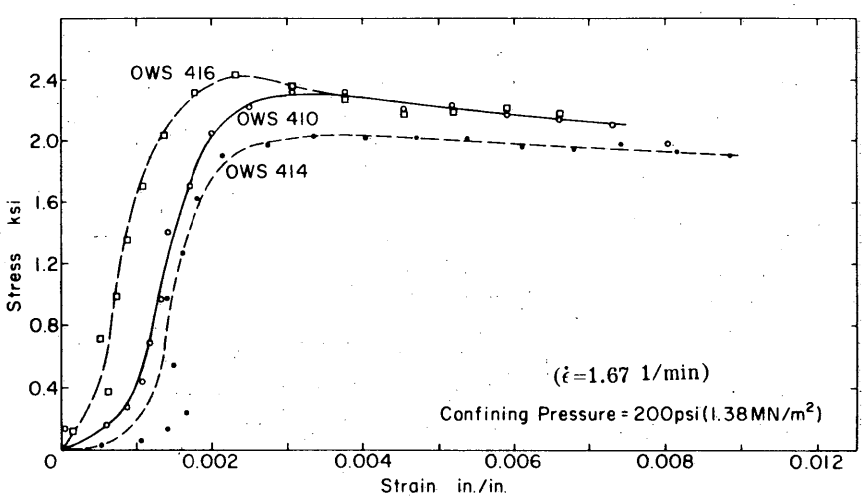
OWS 416
OWS 410
OWS 414
($\dot{\epsilon}$=1.67 1/min)
Confining Pressure = 200psi(1.38MN/m^2)
Stress ksi
2.4
2.0
1.6
1.2
0.8
0.4
0
0.002
0.004
0.006
0.008
0.012
Strain in./in.

B11.

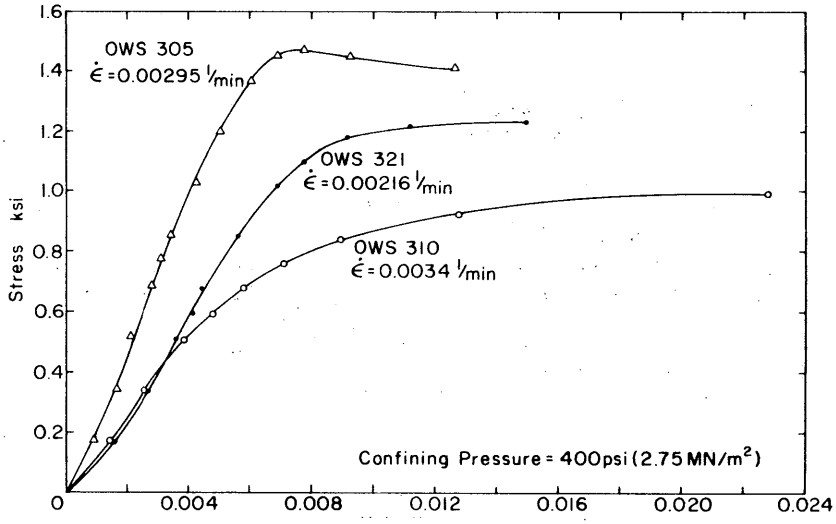
OWS 305
$\dot{\epsilon}$ = 0.00295 1/min
OWS 321
$\dot{\epsilon}$ = 0.00216 1/min
OWS 310
$\dot{\epsilon}$ = 0.0034 1/min
Confining Pressure = 400psi (2.75 MN/m²)
Stress ksi
1.6
1.4
1.2
1.0
0.8
0.6
0.4
0.2
0
0.004
0.008
0.012
0.016
0.020
0.024

B12.

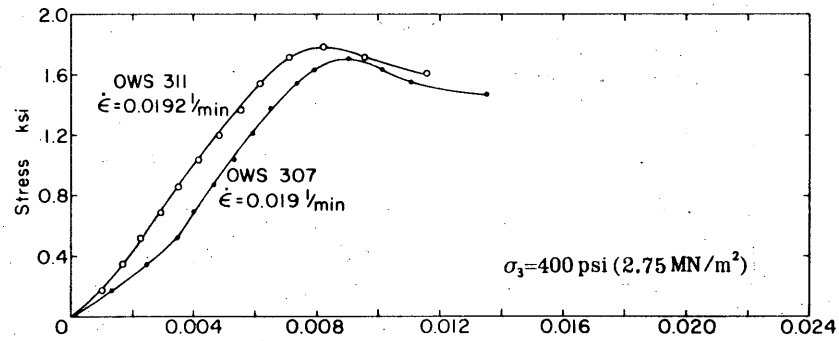
OWS 311
$\dot{\epsilon}$ = 0.0192 1/min
OWS 307
$\dot{\epsilon}$ = 0.019 1/min
σ_3 = 400 psi (2.75 MN/m²)
Stress ksi
2.0
1.6
1.2
0.8
0.4
0
0.004
0.008
0.012
0.016
0.020
0.024

B13.

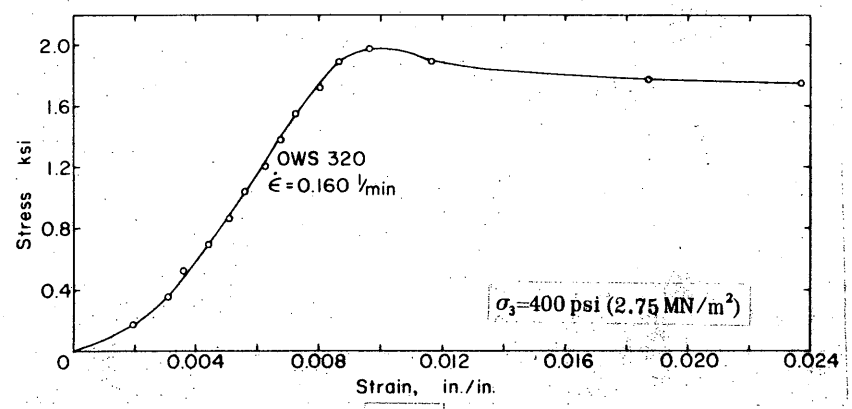
OWS 320
$\dot{\epsilon}$ = 0.160 1/min
σ_3 = 400 psi (2.75 MN/m²)
Stress ksi
2.0
1.6
1.2
0.8
0.4
0
0.004
0.008
0.012
0.016
0.020
0.024
Strain, in./in.

B14.

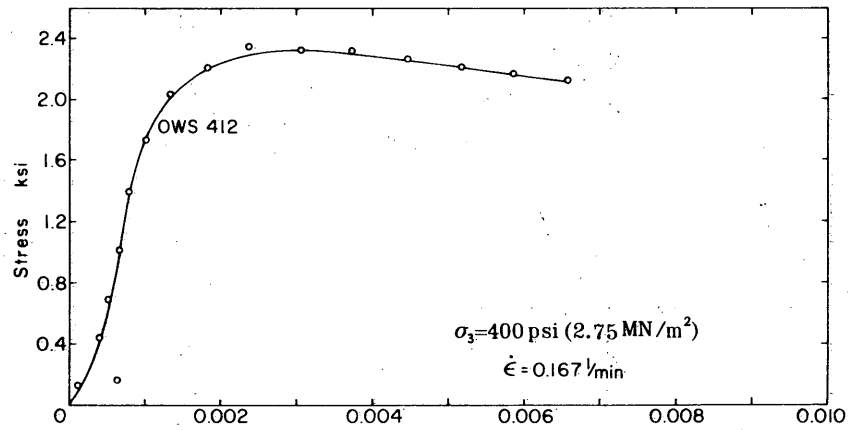
Stress ksi
2.4
2.0
1.6
1.2
0.8
0.4
0
0.002
0.004
0.006
0.008
0.010
OWS 412
σ_3=400 psi (2.75 MN/m^2)
$\dot{\epsilon}$ = 0.167 1/min

B15.

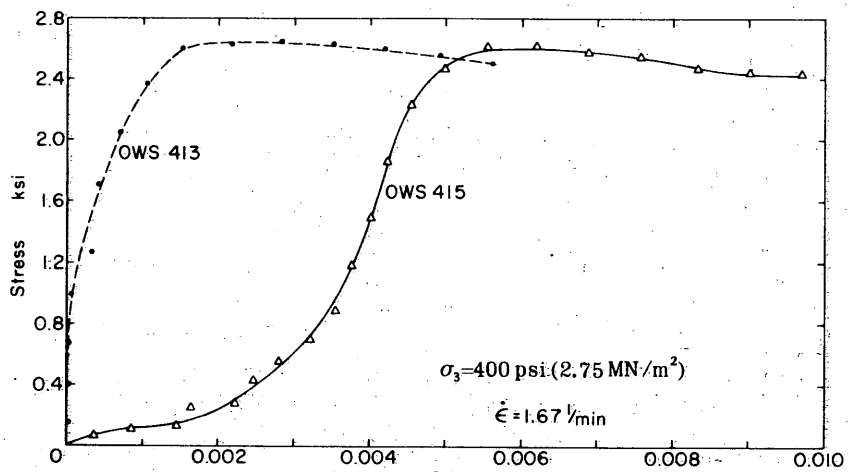
Stress ksi
2.8
2.4
2.0
1.6
1.2
0.8
0.4
0
0.002
0.004
0.006
0.008
0.010
OWS 413
OWS 415
σ_3=400 psi (2.75 MN/m^2)
$\dot{\epsilon}$ = 1.67 1/min

B16.

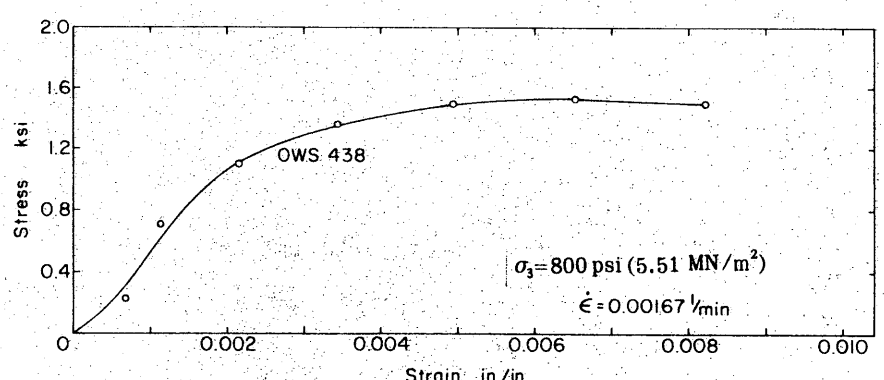
Stress ksi
2.0
1.6
1.2
0.8
0.4
0
0.002
0.004
0.006
0.008
0.010
Strain in./in.
OWS 438
σ_3=800 psi (5.51 MN/m^2)
$\dot{\epsilon}$ = 0.00167 1/min

B17.

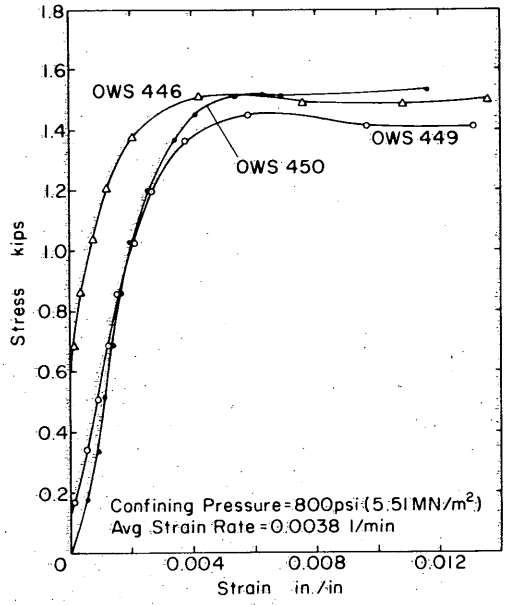
OWS 446
OWS 449
OWS 450
Stress kips
Strain in./in
Confining Pressure=800psi (5.51 MN/m²)
Avg Strain Rate=0.0038 1/min

B18.

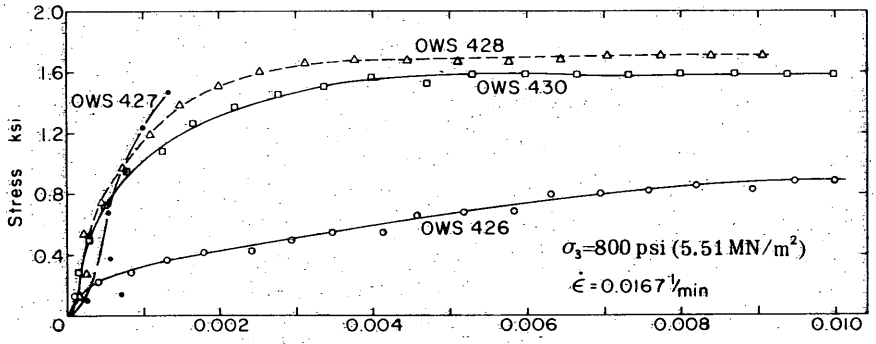
OWS 428
OWS 427
OWS 430
OWS 426
Stress ksi
σ₃=800 psi (5.51 MN/m²)
ε̇ = 0.0167 1/min

B19.

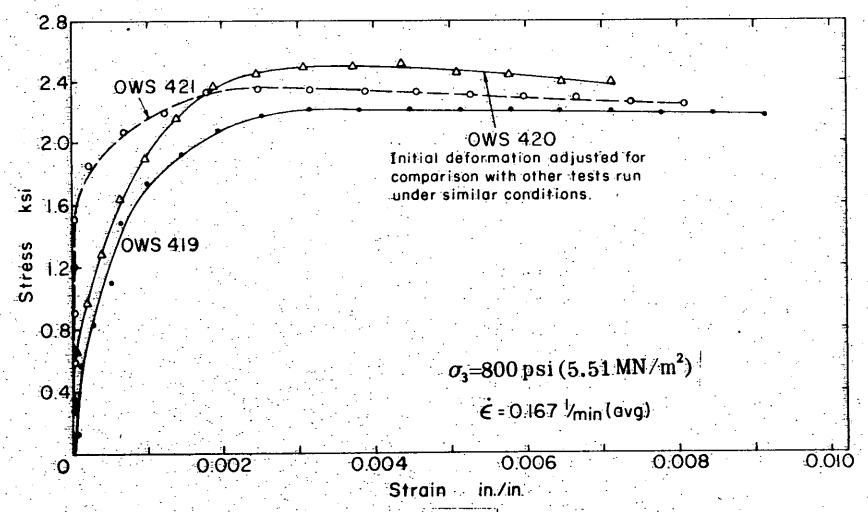
OWS 421
OWS 420
Initial deformation adjusted for comparison with other tests run under similar conditions.
OWS 419
Stress ksi
Strain in./in
σ₃=800 psi (5.51 MN/m²)
ε̇ = 0.167 1/min (avg)

B20.

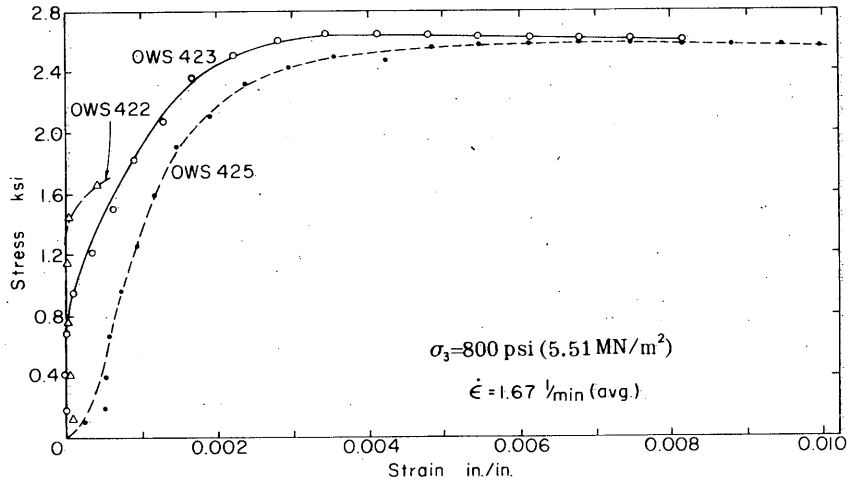
OWS 423
OWS 422
OWS 425
Stress ksi
σ_3=800 psi (5.51 MN/m^2)
$\dot{\epsilon}$ = 1.67 1/min (avg.)
Strain in./in.

B21.

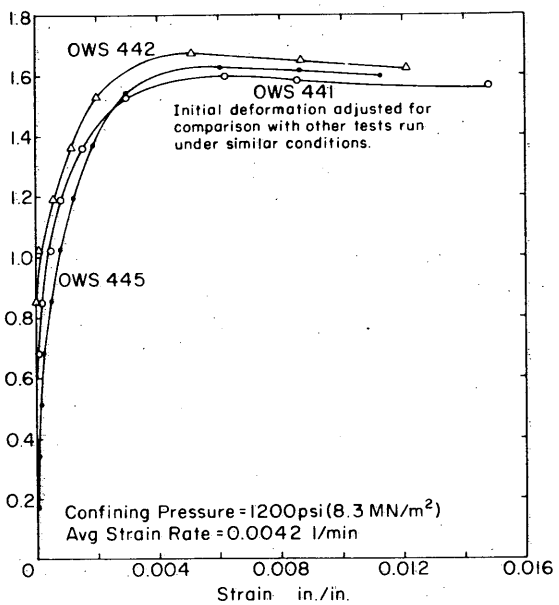
OWS 442
OWS 441
Initial deformation adjusted for comparison with other tests run under similar conditions.
OWS 445
Confining Pressure = 1200psi (8.3 MN/m^2)
Avg Strain Rate = 0.0042 1/min
Strain in./in.

B22.

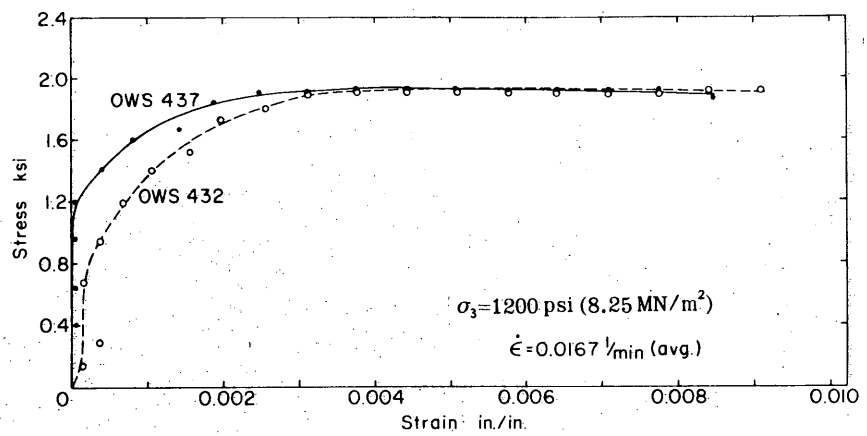
OWS 437
OWS 432
Stress ksi
σ_3=1200 psi (8.25 MN/m^2)
$\dot{\epsilon}$ = 0.0167 1/min (avg.)
Strain in./in.

B23.

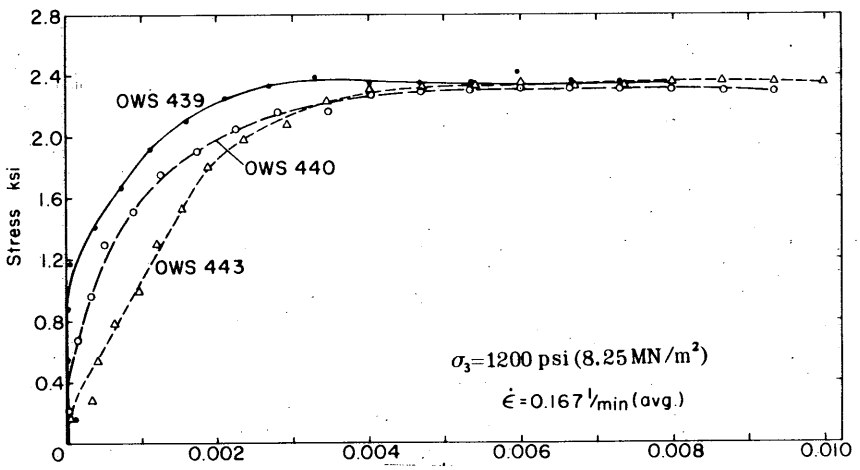
2.8
2.4
2.0
1.6
1.2
0.8
0.4
0
Stress ksi
OWS 439
OWS 440
OWS 443
σ_3=1200 psi (8.25 MN/m^2)
$\dot{\epsilon}$ = 0.167 1/min (avg.)
0.002
0.004
0.006
0.008
0.010

B24.

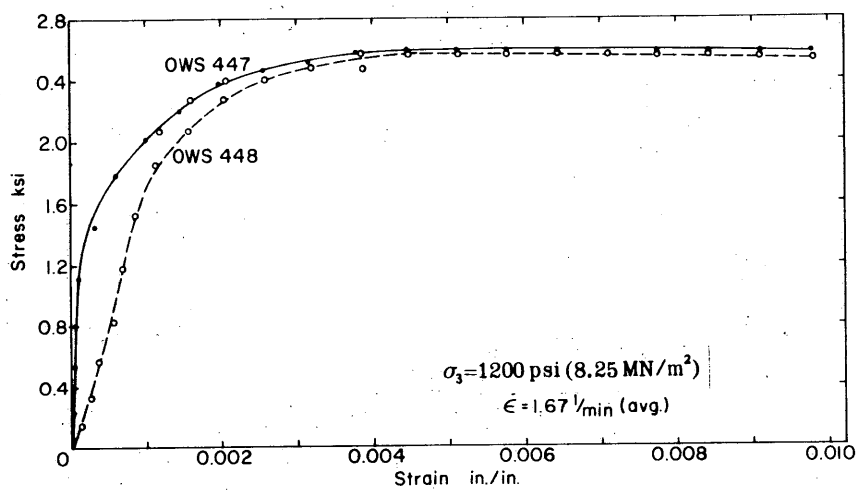
2.8
0.4
2.0
1.6
1.2
0.8
0.4
0
Stress ksi
OWS 447
OWS 448
σ_3=1200 psi (8.25 MN/m^2)
$\dot{\epsilon}$ = 1.67 1/min (avg.)
0.002
0.004
0.006
0.008
0.010
Strain in./in.

B25.

DOCUMENT CONTROL DATA - R & D

Security classification of title, body of abstract and indexing annotation must be entered when the overall report is classified)

1. ORIGINATING ACTIVITY *(Corporate author)*
U.S. Army Cold Regions Research and Engineering Laboratory
Hanover, NH 03755

2a. REPORT SECURITY CLASSIFICATION
Unclassified

2b. GROUP

3. REPORT TITLE
TRIAXIAL CONSTANT STRAIN RATE TESTS AND TRIAXIAL CREEP TESTS ON FROZEN OTTAWA SAND

4. DESCRIPTIVE NOTES *(Type of report and inclusive dates)*

5. AUTHOR(S) *(First name, middle initial, last name)*
Francis H. Sayles

6. REPORT DATE	7a. TOTAL NO. OF PAGES	7b. NO. OF REFS
August 1974	32	12

8a. CONTRACT OR GRANT NO.	9a. ORIGINATOR'S REPORT NUMBER(S)
b. PROJECT NO.	Technical Report 253
c.	9b. OTHER REPORT NO(S) *(Any other numbers that may be assigned this report)*
d.	

10. DISTRIBUTION STATEMENT
Approved for public release; distribution unlimited.

11. SUPPLEMENTARY NOTES	12. SPONSORING MILITARY ACTIVITY
	Directorate of Military Construction Office, Chief of Engineers Washington, D.C.

13. ABSTRACT

Saturated frozen Ottawa sand cylinders and polycrystalline columnar ice were tested in the laboratory under triaxial compressive stress conditions using: 1) constant rate of axial strain, and 2) constant load, i.e. creep tests. The constant rate of axial strain tests were performed by applying axial strain rates in the range from 0.1 to 50% per minute and confining pressures from 0 to 1200 psi (84.4 kg/cm^2). The triaxial compression creep tests were conducted for time periods up to 3000 hr using a range of confining pressures from 0 to 800 psi (56 kg/cm^2) and deviator stresses from 37.5 to 1000 psi (2.6 to 70.3 kg/cm^2). The resulting stress-strain curves and Mohr envelopes for the constant rate of axial strain tests indicate that at rates of strain greater than about 0.02 per minute, the ice matrix fractures prior to the development of friction between the sand grains. At slower rates of applied strain, the friction between sand grains develops, presumably because ice has sufficient time to creep from between the sand grains. The relationship between the observed maximum deviator stress σ and the applied strain rate $\dot{\epsilon}$ can be represented by the empirical expression $\sigma = B\dot{\epsilon}^{\alpha}$ for all the confining pressures tested, where B and α are constants. Results from the triaxial creep tests show that creep strength increases with confining pressure and axial creep strain is reduced by increasing the confining pressure. It is suggested that the long-term ultimate creep strength of saturated frozen sand is a function of the internal friction of the sand which could be determined through triaxial tests on freely drained unfrozen sand.

14. KEY WORDS

Creep properties	Ice	Soil properties
Frozen soils	Permafrost	Soil tests

DD FORM 1 NOV 68 1473 REPLACES DD FORM 1473, 1 JAN 64, WHICH IS OBSOLETE FOR ARMY USE.